A differential equation for approximate wall distance

E. Fares[*,†] and W. Schröder

Aerodynamisches Institut, RWTH Aachen, Wüllnerstrasse zw. 5 und 7, D-52062 Aachen, Germany

SUMMARY

A partial differential equation to compute the distance from a surface is derived and solved numerically. The benefit of such a formulation especially in combination with turbulence models is shown. The details of the formulation as well as several examples demonstrating the influence of its parameters are presented. The proposed formulation has computational advantages and can be favourably incorporated into one- and two-equation turbulence models like e.g. the Spalart–Allmaras, the Secundov or Menter's SST model. Copyright © 2002 John Wiley & Sons, Ltd.

KEY WORDS: wall distance; turbulence modelling

1. INTRODUCTION

In some fields of CFD such as turbulence modelling and grid generation the normal distance to the nearest surface, usually a rigid wall, is required. It is clear that such a calculation can be accurately carried out by calculating the minimum distance between discrete points on the surfaces and the points within the domain of integration. If the grid lines are not orthogonal to the surface, which is the case in unstructured meshes, more time consuming geometrical techniques must be used to compute the exact normal vector on the surface that provides a position to interpolate the normal distance. Such calculations require operations in the order $\mathcal{O}(M \cdot N)$, where M and N represent the number of grid points on the surface and on the whole domain, respectively. This may be regarded as a cheap calculation even though the operations involved include point operations and branches if M is at least one order of magnitude smaller than N, which is usually the case. Considering on the other hand the fact that these operations prevent the use of vector acceleration and require massive communication between the domains on parallel architectures to exchange all grid co-ordinates, such a trivial computation turns out to be complicated and computationally expensive, in particular for large problems.

---

[*] Correspondence to: E. Fares, Aerodynamisches Institut Aachen, RWTH Aachen, Wüllnerstrasse zw. 5 und 7, D-52062 Aachen, Germany.
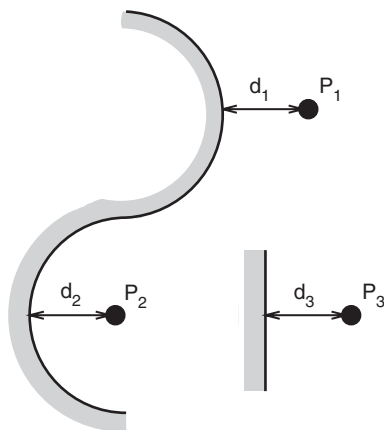[†] E-mail: ehab@aia.rwth-aachen.de

Figure 1. Example of equal distances.

Considering the formulations of current turbulence models like the Baldwin and Lomax [1], Baldwin–Barth [2], Spalart–Allmaras [3], Secundov's v_{t92} [4] and Menter's SST [5] model it is apparent, that the near-wall turbulence is often considered in the formulations by explicitly enforcing a dependence of the production or destruction terms, e.g. wall damping terms, on the normal distance d to the nearest wall or on the normalized distance $y^+ = u_\tau d/v$.

Since all these models include empirical constants the model has to be tuned for the near wall turbulence, which is usually done for the zero pressure gradient boundary layer or slightly curved surfaces. This procedure is not exact for all kinds of geometries where strong curvature is expected. The question arises whether a different formulation of the distance can be found, that can take curvature effects at strong curved surfaces as well as sharp edges and corners into account while preserving the results for the flat plate. This is motivated by the idea that an exact computation of the distance leads to the same result of the distance $d_1 = d_2 = d_3$ for the convex/concave and plane surfaces shown in Figure 1. Even though the points P_1, P_2, P_3 have the same wall distance they possess a different near-wall impact in many turbulence models. Hence, a physically more relevant choice would be $d_1 < d_3 < d_2$ to express the increase or decrease in wall influence at convex or concave curved surfaces. The same is valid for sharp corners or edges, with additionally smoothing the undesired crisp distribution of the exact distance.

Those two drawbacks, parallelization disadvantages and non-physically based influence, can be remedied by replacing the regular normal wall distance d by a suitable distribution $\mathscr{D}$. We seek a new distance function $\mathscr{D}$ that can be numerically determined by methods similar to those used for the numerical flow solutions. Additionally, $\mathscr{D}$ should be adjustable for a better behaviour of turbulence models that require this distance concept at curved surfaces and corners.

A proposal of such a formulation can be found in References [6, 7] which was derived from a modified Poisson equation. Several arguments and weighting factors have to be evaluated to identify the nearest surface and locate the nearest corner and gap orientation. This equation

was used in conjunction with a variety of turbulence models in isothermal flows around electronic components. Unfortunately, details about the derivation of this equation, boundary conditions as well as the solution procedure and the ability to control the deviation from the exact distance, e.g. smoothing at sharp edges, were not thoroughly discussed.

Another coupling of a newly formulated distance equation with the Spalart–Allmaras turbulence model was introduced in References [8, 9] leading to qualitatively good results in two- and three-dimensional flows. In this paper a detailed presentation of this proposed distance function will be given. A partial differential equation is derived in the next section followed by recommendations for the numerical solution and suitable initial and boundary conditions. Finally, examples are discussed to point out the ability of the equation to meet the desired requirements and to present reference solutions to allow the tuning wished by researchers in the field of turbulence modelling. The appendix summarizes all relevant equations and is provided for implementation purposes.

2. DERIVATION OF THE EQUATION

The distance function $\mathscr{D}$ for a three-dimensional space is derived from the requirement that the gradient of such a function has norm 1 [10]

$$|\mathrm{grad}(\mathscr{D})| = |(\mathscr{D}_x, \mathscr{D}_y, \mathscr{D}_z)^{\mathrm{T}}| = 1 \tag{1}$$

$$\Rightarrow (\mathscr{D}_x)^2 + (\mathscr{D}_y)^2 + (\mathscr{D}_z)^2 = 1 \tag{2}$$

which is actually the requirement that the function $\mathscr{D}$ has a linear solution. The second condition is that the gradient of $\mathscr{D}$ should be normal to the surface. This is automatically fulfilled by enforcing the Dirichlet boundary condition on the surface

$$\mathscr{D}_{\mathrm{wall}} = \mathscr{D}_0 = \mathrm{const.} \tag{3}$$

If the gradient had a non-orthogonal orientation, a tangential component on the surface would exist. Such a component would contradict either the constant boundary condition or the constant norm of the gradient. The validity of the above formulation can be analytically verified for trivial geometries, say, a plane or a sphere.

Note, however, that the iterative numerical solution of the distance equation (2) has some drawbacks:

- The initialization of the distribution at the beginning of the calculation by a large constant value will lead to a non-zero residual, even when all boundary conditions are turned off. Only a linear distribution in one direction fulfils the equation. Compared with an initialized parallel flow it seems favourable to have an initialization of the distance equation that indicates convergence either globally or at least locally if there is no wall in the domain or it is far away, respectively.
- The information about the existence of the surfaces must propagate through the whole computational domain to attain the linear distribution. This can be avoided, since the dependence on the distance d in almost all cases is only important in the vicinity of the surfaces involved. That is, there is no need to extend this requirement globally.

- If the integration domain is not bounded by walls there is no suitable distribution of the distance function possible except for the infinite value $\mathcal{D} \to \infty$, which should be avoided numerically.

Therefore, Equation (2) is reformulated to overcome these difficulties by substituting the function $\mathcal{D}$ by its inverse $\mathcal{G} = 1/\mathcal{D}$

$$(\mathcal{G}_x)^2 + (\mathcal{G}_y)^2 + (\mathcal{G}_z)^2 = \mathcal{G}^4$$

$$\Rightarrow |\text{grad}(\mathcal{G})|^2 = \mathcal{G}^4 \tag{4}$$

$$\mathcal{G}_{\text{init}} = 0.0 \tag{5}$$

$$\mathcal{G}_{\text{wall}} = 1/\mathcal{D}_0 = \mathcal{G}_0 \tag{6}$$

To avoid infinite values $\mathcal{D}_0$ should not be equal to zero in the boundary condition (6) if it is evaluated explicitly at the boundary. This issue will be addressed below. The initial distribution in the interior domain is given by Equation (5), which represents a trivial solution of Equation (4). The term $|\text{grad}(\mathcal{G})|^2$ is rearranged using the identity

$$(\mathcal{G} \cdot \mathcal{G}_x)_x = (\mathcal{G}_x)^2 + \mathcal{G} \cdot \mathcal{G}_{xx}$$

for each component of the term to attain an elliptical formulation that is easier to solve numerically

$$(\mathcal{G} \cdot \mathcal{G}_x)_x + (\mathcal{G} \cdot \mathcal{G}_y)_y + (\mathcal{G} \cdot \mathcal{G}_z)_z - \mathcal{G} \cdot (\mathcal{G}_{xx} + \mathcal{G}_{yy} + \mathcal{G}_{zz}) - \mathcal{G}^4 = 0 \tag{7}$$

where $(\mathcal{G}_{xx} + \mathcal{G}_{yy} + \mathcal{G}_{zz})$ represents a Laplacian operator of $\mathcal{G}$. To have the desired possibility of tuning the distance function near edges and corners an elliptic term $\sigma \cdot \mathcal{G}(\mathcal{G}_{xx} + \mathcal{G}_{yy} + \mathcal{G}_{zz})$ is added. Here, the quantity σ must be positive since the introduced term resembles a diffusion term, which must be mathematically and physically positive ($\mathcal{G}$ is also always positive). The impact of this parameter σ on the solution will be thoroughly discussed in the following sections. The source term $\mathcal{G}^4$ is multiplied by the factor γ to compensate for the newly added elliptic term. The final equation reads

$$(\mathcal{G} \cdot \mathcal{G}_x)_x + (\mathcal{G} \cdot \mathcal{G}_y)_y + (\mathcal{G} \cdot \mathcal{G}_z)_z + (\sigma - 1) \cdot \mathcal{G} \cdot (\mathcal{G}_{xx} + \mathcal{G}_{yy} + \mathcal{G}_{zz}) - \gamma \cdot \mathcal{G}^4 = 0 \tag{8}$$

where $\sigma > 0$ extends the elliptic character of the equation and, as we will show below, determines the smoothing of the distance function at the corners. Since the introduction of σ changes the inverse linear behaviour of the distance function $\mathcal{G}$ the value of γ is chosen to account for the newly introduced additional smoothing and compute the exact solution for the plane. In doing so no changes to the formulations of the turbulence models using the distance concept are necessary. A plane in three dimensions has a constant normal vector $\mathbf{n}_0$ that can be defined by two angles α and β. Using the exact inverse distance function $\mathcal{G}$

$$\mathcal{G} = \frac{1}{x \cos(\alpha) \cos(\beta) + y \cos(\alpha) \sin(\beta) + z \sin(\beta) + \mathcal{D}_0} \tag{9}$$

in Equation (8) yields for γ

$$\gamma = (1 + 2 \cdot \sigma) \tag{10}$$

Inserting this linear relation between γ and σ into Equation (8) leads to no deviation for the plane and a deviation of $\mathcal{O}(\sigma/(r^2 + \sqrt{r} \cdot (\mathcal{D}_0 + r_0)^3))$ between the exact and the proposed inverse distance for a sphere, where r is the distance from the sphere centre and r_0 the radius of the sphere.

3. NUMERICAL SOLUTION

In this paper, the numerical algorithm to solve the proposed equation is presented in a structured multi-block framework. Other possibilities of the discretization using higher-order schemes as well as approximations on unstructured grids will be discussed elsewhere. Due to the elliptic character the terms of the equations are discretized using central differences based on 3 point stencils in each direction. Details of the discretization are given in the appendix.

3.1. Boundary conditions

The initial distribution $\mathcal{G}_{\text{init}} = 0$ resembles the free stream solution. It is an exact solution of the equation in the interior and yields also a good approximation at the far field boundaries. Since the quantity $\mathcal{G}$ grows inversely with the distance, strong gradients are expected only in the near-wall region, which is exactly where the distance calculation is needed in the usual turbulence models.

The boundary condition at the wall $\mathcal{G}_{\text{wall}} = \mathcal{G}_0$ can be theoretically chosen according to the requirements of the turbulence model. The ν_{t92} model of Secundov [4] for example reduces the distance to the nearest wall d by the quantity k_s $(d_{\text{eff}} = d_w + 0.01 k_s)$ to account for wall roughness. A modified Spalart–Allmaras model for rough wall boundary layers is proposed in Reference [11] which also shifts the distance d by the value $R = 0.9(\nu/u_\tau)[\sqrt{k_s^+} - k_s^+ \exp(-k_s^+/6)]$ where $k_s^+ = k_s u_\tau/\nu$ represents the normalized roughness. It should be noted that the eddy viscosity is also enlarged at the rough wall. Therefore, the obtained effect can be interpreted as a shift of the near-wall velocity profile towards the wall of the order $\mathcal{O}(y^+)$ leading to an increase of the skin friction.

If the integration domain of a turbulent flow calculation contains many objects of different sizes, e.g. a very thin wire in the turbulent channel flow within the boundary layer, there will be insignificant influence of the thin wire on the production or dissipation of the turbulent viscosity at the channel wall and therefore on the skin friction distribution. Note, that this is not to be confused with a tripping wire used to enforce transition. Depending on the influence of the object a suitable value of $\mathcal{G}_0$, e.g. based on the reference size, can be chosen. This feature will be addressed in the examples below. Practically on the other hand a choice of $\mathcal{G}_0 \approx 1.0/x_{\text{ref}}$ seems to be appropriate since this would limit the range of the non-dimensional value of $\mathcal{G}$ between 0 and 1 thereby avoiding large values near the wall, where the exact inverse distance $1/d$ reaches infinity at the wall. Since the value of $\mathcal{G}$ goes directly into the source term $\gamma \mathcal{G}^4$ a strong gradient near the wall will also be avoided by the proposed offset $\mathcal{G}_0$ which will not only lead to a better numerical stability but also enables the use of coarse grids even near the wall.

The numerical boundary condition at the far field boundaries can be formulated according to the assumption that $\mathcal{G}$ or $\partial_n \mathcal{G}$ approximately vanishes. These simple boundary conditions, however, have physical limitations. For this reason we introduce a more accurate

formulation

$$\mathbf{r}_{\mathrm{b}} = \mathbf{r}_{ijk} = (x_{\mathrm{b}} \quad y_{\mathrm{b}} \quad z_{\mathrm{b}})^{\mathrm{T}} \tag{11}$$

$$\mathbf{r}_{\mathrm{in}} = \mathbf{r}_{i\pm 0/1 j\pm 0/1 k\pm 0/1} = (x_{\mathrm{in}} \quad y_{\mathrm{in}} \quad z_{\mathrm{in}})^{\mathrm{T}} \tag{12}$$

$$\Delta r = |\mathbf{r}_{\mathrm{b}} - \mathbf{r}_{\mathrm{in}}| \tag{13}$$

$$\mathscr{G}_{\mathrm{b}} = \frac{\mathscr{G}_{\mathrm{in}}}{1 + \mathscr{G}_{\mathrm{in}} \cdot \Delta r} \tag{14}$$

where $\mathbf{r}_{\mathrm{in}}$ represents the first inner point from the far field boundary and $\mathbf{r}_{\mathrm{b}}$ is the location of the boundary. This boundary condition shifts the exact calculation of the inverse distance from the interior of the integration domain onto the boundary. The only requirement is that the first inner point is in the direction of the gradient of $\mathscr{G}$. To avoid calculating the exact direction of the gradient of $\mathscr{G}$ at the boundary a multi-dimensional linear extrapolation can be used for the distance distribution. The exact description is given in the appendix.

3.2. Integration scheme

The iterative solution process can be explicitly advanced in an artificial time with c_{r} being a relaxation factor

$$\mathscr{G}_t = c_{\mathrm{r}} \cdot [(\mathscr{G} \cdot \mathscr{G}_x)_x + (\mathscr{G} \cdot \mathscr{G}_y)_y + (\mathscr{G} \cdot \mathscr{G}_z)_z + (\sigma - 1) \cdot \mathscr{G} \cdot (\mathscr{G}_{xx} + \mathscr{G}_{yy} + \mathscr{G}_{zz}) - \gamma \cdot \mathscr{G}^4] \tag{15}$$

Note that the equation loses its dimensional consistency unless c_{r} is appropriately chosen. The form of Equation (15) resembles a transport equation that can be implemented into existing numerical algorithms as an extension of the turbulence models.

However, numerical stability investigations show that an explicit integration has strong limitations on the time steps due to non-linearities that cannot be analysed analytically. Therefore, a more superior Newton type implicit calculation was carried out. The scheme is described here for the one-dimensional case

$$\mathscr{R}^{(n)} = (\mathscr{G} \cdot \mathscr{G}_x)_x + (\sigma - 1) \cdot \mathscr{G} \cdot (\mathscr{G}_{xx}) - \gamma \cdot \mathscr{G}^4 \tag{16}$$

$$\mathscr{G}^{(n+1)} = \mathscr{G}^{(n)} - c_{\mathrm{r}} \mathscr{J}^{(n)^{-1}} \mathscr{R}^{(n)} \tag{17}$$

The Jacobian $\mathscr{J}_{ij} = \partial \mathscr{R}_i / \partial \mathscr{G}_j$ is given explicitly in the appendix. The matrix $\mathscr{J}$ has a tridiagonal structure for structured grids. It can be inverted using e.g. a tridiagonal Gaussian elimination of order $\mathscr{O}(N)$. It was found that this integration scheme is highly efficient and robust for $\sigma \gtrless 0.2$ using the numerical boundary conditions given in Equations (5), (6) and (14). Two special cases for σ can be derived for $\sigma = 1$ and $\sigma \to \infty$. The Laplacian operator in Equation (8) disappears for $\sigma = 1$. The limit $\sigma \to \infty$ reduces Equation (15) to a simple equation

$$\sigma \to \infty: \quad \mathscr{G}_{xx} + \mathscr{G}_{yy} + \mathscr{G}_{zz} - 2\mathscr{G}^3 = 0 \tag{18}$$

At values σ less than 0.2 numerical instabilities of the scheme occur. If the relaxation factor is determined using $c_{\mathrm{r}} \approx 1.0/\max(\Delta x_i/\Delta x_{i-1})$ a stable and efficient behaviour for stretching factors $\max(\Delta x_i/\Delta x_{i-1})$ up to 5.0 is achieved. For the case of the flat plate $\mathscr{O}(10)$ iterations were necessary to obtain a converged solution.

The multi-dimensional problem is solved by splitting the Jacobian $\mathscr{J}$ into a diagonally dominant part and the off-diagonal part where the diagonal part includes the contributions of all directions. That is

$$\mathscr{J} = \mathscr{J}_{x+\text{diag}} + \mathscr{J}_{y-\text{diag}} + \mathscr{J}_{z-\text{diag}} \tag{19}$$

means that $\mathscr{J}_{y-\text{diag}}$ and $\mathscr{J}_{z-\text{diag}}$ have zero diagonals.

Following Equation (17) the Newton iteration can be performed by the approximation

$$\Delta \mathscr{G}^{(n+1)} = -c_{\text{r}}(\mathscr{J}_{x+\text{diag}}^{(n)})^{-1}[\mathscr{R}^n + \mathscr{J}_{y-\text{diag}}^{(n)} + \mathscr{J}_{z-\text{diag}}^{(n)})\Delta \mathscr{G}^{(n)}] \tag{20}$$

The advantage of this splitting is that all the sub Jacobians are tridiagonal, if they are re-ordered conveniently, such that the inversion and the multiplication stay of $\mathscr{O}(N)$. Numerical experience indicates that the terms $(\mathscr{J}_{y-\text{diag}} + \mathscr{J}_{z-\text{diag}})\Delta \mathscr{G}^{(n)}$ can be neglected in favour of the dominant term $\mathscr{R}^n$, which simplifies the method even further.

To avoid propagation of information in one preferred direction all diagonally dominant Jacobians are considered and averaged

$$\mathscr{R}_x^{(n)} = (\mathscr{J}_{x+\text{diag}}^{(n)})^{-1}\mathscr{R}^{(n)} \tag{21}$$

$$\mathscr{R}_y^{(n)} = (\mathscr{J}_{y+\text{diag}}^{(n)})^{-1}\mathscr{R}^{(n)} \tag{22}$$

$$\mathscr{R}_z^{(n)} = (\mathscr{J}_{z+\text{diag}}^{(n)})^{-1}\mathscr{R}^{(n)} \tag{23}$$

$$\Delta \mathscr{G}^{(n+1)} = -c_{\text{r}}/3(\mathscr{R}_x^{(n)} + \mathscr{R}_y^{(n)} + \mathscr{R}_z^{(n)}) \tag{24}$$

Of course, other schemes for the solution of the equation using other iterative methods like ILU, CGSTAB or GMRES and combinations with multigrid acceleration are possible.

4. EXAMPLES

The equation just derived is solved numerically for various one- and two-dimensional cases that explain the influence of the free parameters on the distance calculation and present relevant examples of edges and curved surfaces including a realistic 3-element airfoil configuration. The one-dimensional examples are documented in detail and approximations of relevant functions are given to allow further tuning of the parameters in conjunction with turbulence models.

Finally, three-dimensional calculations of different block sizes and numbers are presented showing the benefit of the proposed numerical solution and yielding theoretical aspects of expected computational times.

4.1. One-dimensional case

The numerical solution of the one-dimensional equation with one end defined as a wall and the other as a far field resembling a flat plate meets the exact distance for all σ chosen, which is one of the requirements of the derived equation.
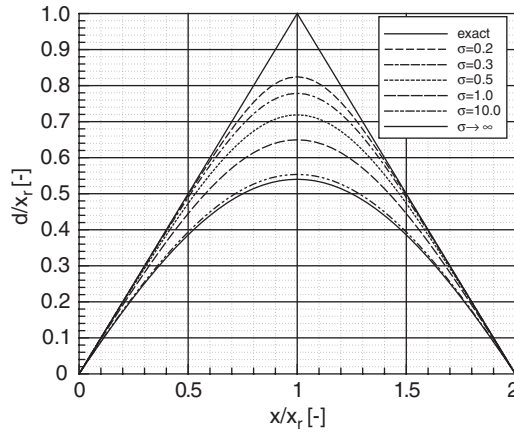
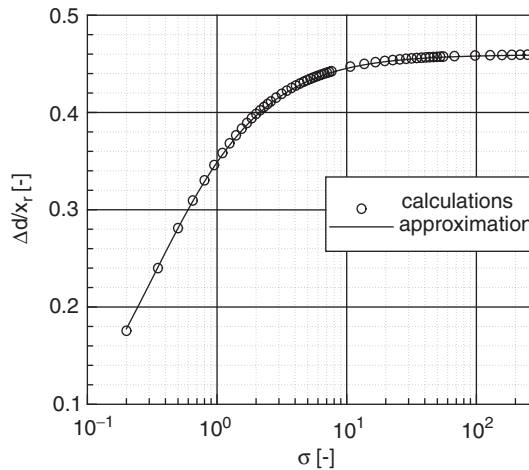Figure 2. Exact and calculated distance for different σ.

Figure 3. Approximation of the deviation Δd for different σ.

When the wall boundary condition ($\mathscr{G}_0 = 1.0, x_{\text{ref}} = 1.0$) is enforced at both ends, which resembles a channel, the maximum deviation Δd from the exact distance occurs in the middle at $x/x_r = 1$ as seen in Figure 2.

The desired smoothing is controlled by the value of σ, where a larger value means a stronger smoothing. The difference $\Delta d = d_{\text{exact}} - d_{\text{calculated}}$ computed for different values of σ is shown in Figure 3. A logarithmic growth of Δd is evidenced having a limit of the deviation for $\sigma \to \infty$. The curve can be approximated by the function

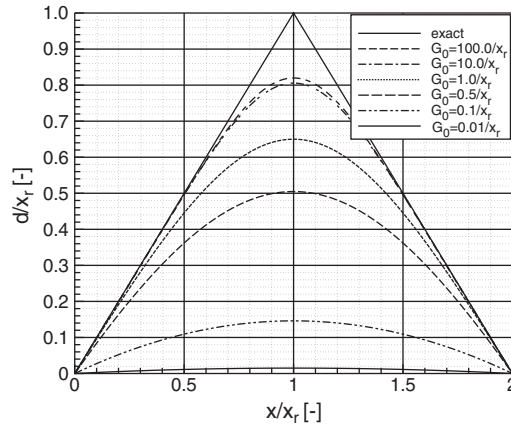$$f(\sigma)_{\text{approx.}} = a \cdot \tanh(b \cdot \ln(1.0 + c \cdot \sigma)) \tag{25}$$

Figure 4. Exact and calculated distance for different $\mathscr{G}_0$ and $\sigma = 1.0$.

with

$$a = \lim_{\sigma \to \infty} \Delta d \approx 0.459, \quad b \approx 0.50, \quad c \approx 6.3 \tag{26}$$

It is worth noting that the value of the wall boundary condition $\mathscr{G}_{\text{wall}} = \mathscr{G}_0 = 1.0/x_{\text{ref}}$ influences the smoothing, too. Since the scalar Equation (8) has only one dimension of the length, the dimensional form of the equation is equivalent to the non-dimensional form, if x and $\mathscr{G}$ are non-dimensionalized with the same reference length x_{ref}. The only situation where the value of x_{ref} is relevant is the definition of the initial and boundary conditions $\mathscr{G}_{\text{init}}$ and $\mathscr{G}_{\text{wall}}$. In the case of the one-sided wall, that is similar to the flat plate in two-dimensions, this numerical value does not play a role, since the solution is the exact distance for all σ and $\mathscr{G}_0$ chosen. For the case of the two-sided wall, simulating a channel in two-dimensions, the exact distance is not fulfilled and there is a maximum smoothing midway between the walls. Figure 4 shows the distributions at various $\mathscr{G}_0$ values for $\sigma = 1.0$. A small $\mathscr{G}_0$ means a greater distance from the wall and as such a stronger deviation from the inverse linear behaviour is observed. It is apparent, that the value at the wall has a profound influence on the calculated inverse distance by controlling the region of the inverse linear behaviour. The difference $\Delta d = d_{\text{exact}} - d_{\text{calculated}}$ calculated for different values of $\mathscr{G}_0$ is presented in Figure 5. There is also a logarithmic behaviour of Δd depending on $\mathscr{G}_0$ and a limit of the deviation for $\mathscr{G}_0 \to 0$. The curve can be approximated by the function

$$\tilde{\mathscr{G}}_0 = \mathscr{G}_0 \cdot x_{\text{ref}} \tag{27}$$

$$f(\tilde{\mathscr{G}}_0)_{\text{approx}} = 1 + a \cdot (\tanh(b \cdot \ln(c \cdot \tilde{\mathscr{G}}_0)) - 1) \tag{28}$$

with

$$a \approx 0.41, \quad b \approx -0.61, \quad c \approx 2.86 \tag{29}$$

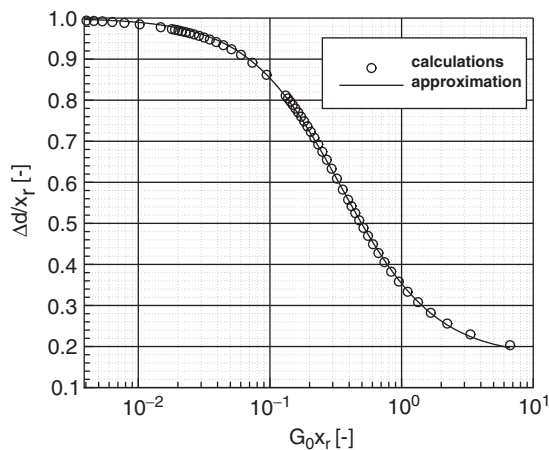$$\lim_{\tilde{\mathscr{G}}_0 \to 0} f(\tilde{\mathscr{G}}_0)_{\text{approx.}} = 1.0 \tag{30}$$

Figure 5. Approximation of the deviation Δd for different $\mathscr{G}_0$.

4.2. Two-dimensional case

4.2.1. Convex/concave corner. In the following example 90° convex and concave corners are investigated, respectively. The calculation is conducted for a range of the parameters σ and $\mathscr{G}_0$ to demonstrate their influence on the solution. The results are compiled in Figure 6.

As in the one-dimensional case a small value of σ and a large value of $\tilde{\mathscr{G}}_0$ yields a better approximation of the exact distance. The most important feature is the smoothing at the corner from both sides, leading to a smaller distance on the concave side and a greater distance on the convex side. The contours do not represent the exact distance. A small spacing between the contours of the distance in Figure 6 like that on the convex side represents a greater calculated distance than the exact distance and a greater spacing as on the concave side represents a smaller distance. In other words, clustered isolines evidence a stronger and separated contours a weaker increase than the exact distance. Note the behaviour at the boundaries using the proposed boundary condition for the case of $\tilde{\mathscr{G}}_0 = 10.0$. The far field boundary condition (14) expects an inverse linear behaviour of $\mathscr{G}$. This is not exactly fulfilled at all boundaries especially in the smoothed interior of the concave corner. Nevertheless, the boundary condition is still performing well and is very effective in cases where the orthogonality of the grid lines is not satisfied at the boundary.

4.2.2. Ellipse. A smoothly curved surface similar to that of an airfoil is represented by an ellipse where the outer and inner part can be investigated. The calculated distance for $\sigma = 1.0$ and $\tilde{\mathscr{G}}_0 = 1.0$ is compared with the exact distance in Figure 7. The same behaviour is encountered as in the above mentioned examples for the concave and convex corner. The investigation of the direct vicinity of the surface, that is presented in Figure 8 for a cut through the axis of the ellipse, shows that the curvature and smoothing effect is observed up to the surface and is stronger on the inner part. Regarding on the other hand distances close to the surface, e.g. in a region of a boundary layer of a high Reynolds number flow in the $\mathcal{O}(y^+)$, the deviations are negligible.
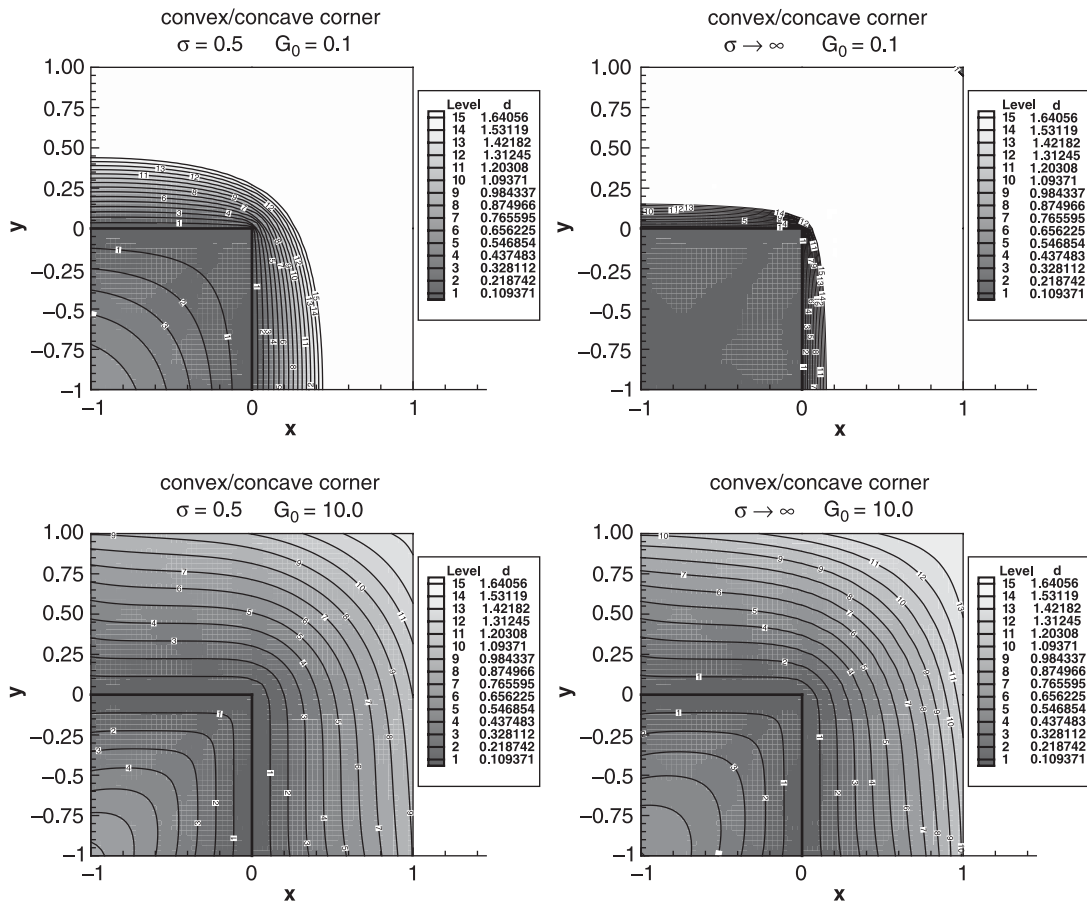
Figure 6. Calculated distance at a convex/concave corner for different values of σ and $\tilde{\mathcal{G}}_0 = \mathcal{G}_0 \cdot x_{\mathrm{ref}}$.

4.2.3. Cylinder in channel. A variation of the wall boundary condition $\mathcal{G}_0$ on different objects within the same integration domain is presented in the following example. A cylinder is given different values of $\mathcal{G}_0$ whereas the value on the channel wall is kept constant $\tilde{\mathcal{G}}_0 = 1.0$. As seen in Figure 9 the object with the higher value of $\tilde{\mathcal{G}}_0$ dominates the calculation of the distance. This parameter is therefore not merely determined by the reference length of the computation for non-dimensional purposes but allows to control various influences of different walls if desired.

4.2.4. Three-element airfoil. The example presents the behaviour of the proposed distance equation for a three-element airfoil BAC 3-11 [12]. The structured grid shown in Figure 10 was successfully used in former calculations [9]. The exact distance based on the calculation of the smallest distance between the grid points within the integration domain and the boundary points on the wall is presented in Figure 11. Note the relatively sharp distribution
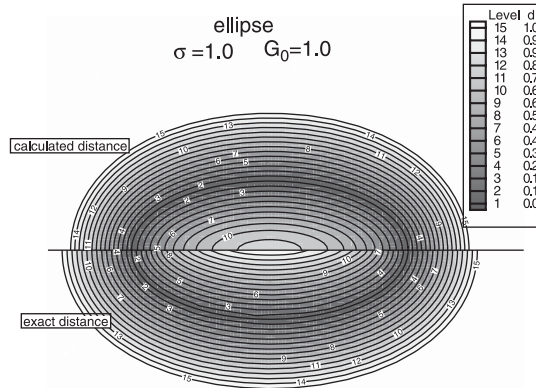
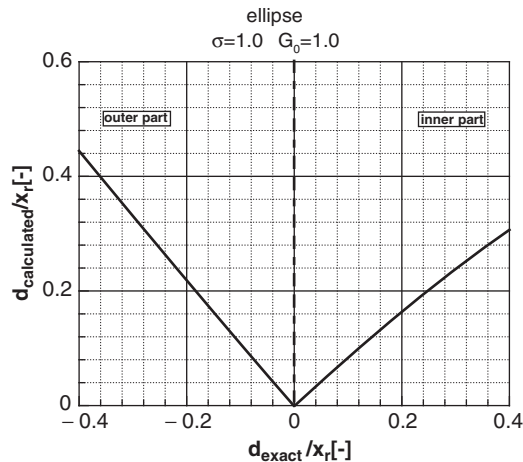Figure 7. Exact and calculated distance for the ellipse.

Figure 8. Deviation of calculated and exact distance at the surface of the ellipse.

in the vicinity of the slat and flap, that results in perturbations in the numerical computation of the turbulent flow. The distance calculation based on the proposed differential equation in Figure 12 shows a comparatively smooth distribution. The computation of this complex topology needed less than 200 iterations to achieve a reduction of 5 orders of magnitude for the residual.

4.3. Three-dimensional case

4.3.1. Single block. To discuss the computational time needed for the proposed calculation juxtaposed to the exact determination of distance the simple cube is considered. It consists of N grid points and has $M \sim N^{2/3}$ points on the boundary. Any exact calculation would
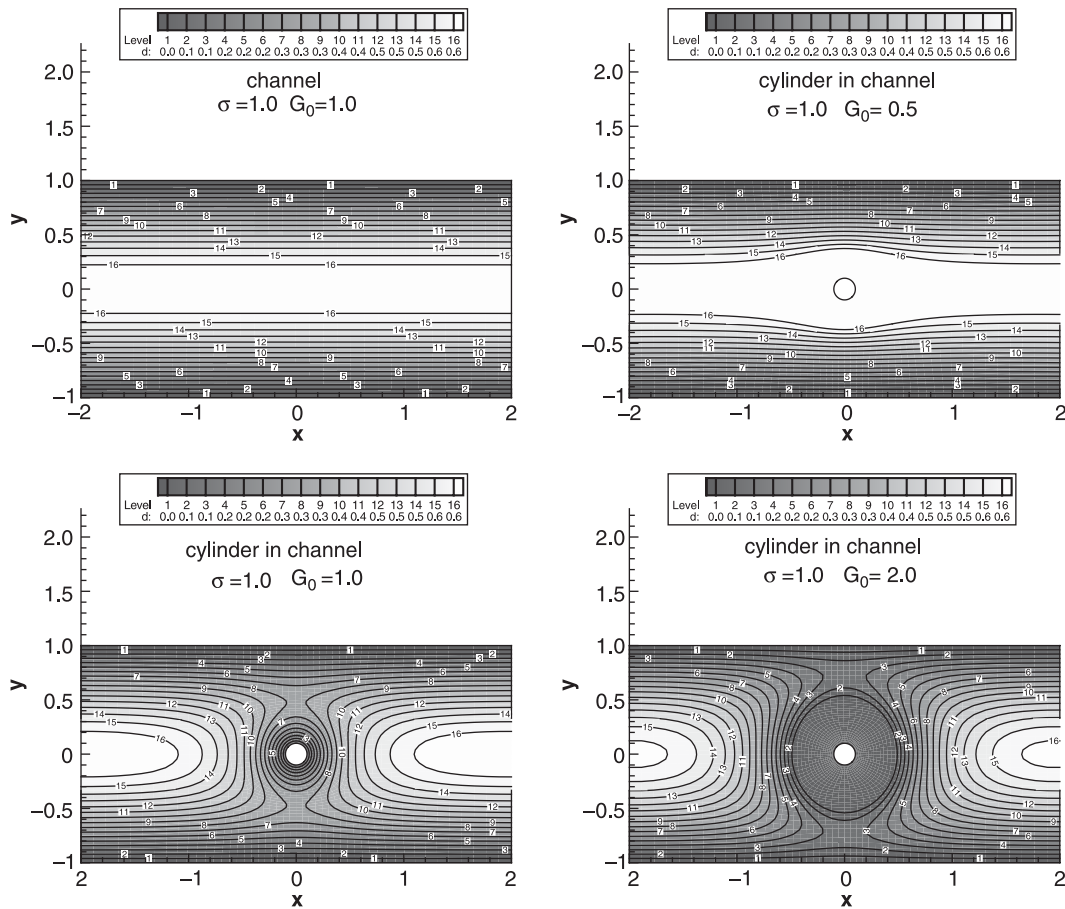
Figure 9. Calculated distance of channel and object with different values of $\mathscr{G}_0$.

need a number of operations of order $\mathcal{O}(N^{5/3})$. A computation based on the partial differential equation is of order $\mathcal{O}(N \cdot \text{it})$, where it represents the number of iterations needed to achieve a converged solution. Within one iteration $\mathcal{O}(N)$ operations are required for the inversion of the tridiagonal matrix. Figure 13 presents the computational time needed for the exact calculation and the computational time required for the convergence of the numerical method, which is defined by a drop of $\mathcal{O}(7)$ magnitudes of the residual. The numerical scheme shows an increase in the number of iterations ranging from $\text{it} = 19$ for $N = 729$ to $\text{it} = 63$ for $N = 7 \times 10^5$. If it is considered to be proportional to N^a then for large N the quantity a is smaller than $\frac{1}{3}$.

4.3.2. Multi block. When the computational domain is divided into several subdomains new boundaries are introduced having B grid points. If the total number of grid points N is equally divided into K subdomains then B can be approximated by $B \sim (N/K)^{2/3}$. The total time for the calculations consists of the communication time T_{comm} needed to exchange values between
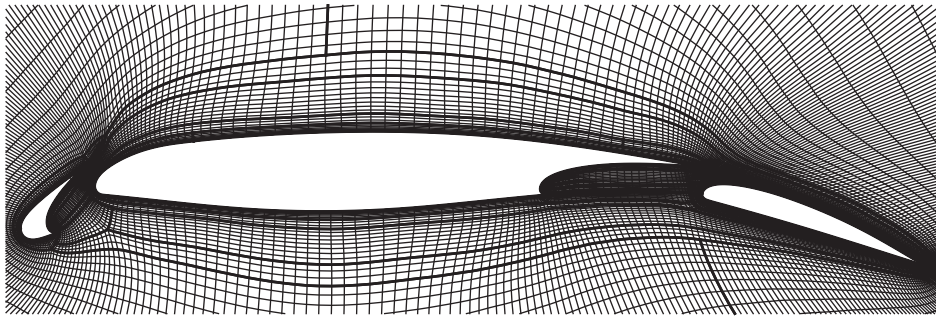
Figure 10. Grid of three-element airfoil consisting of 45 000 grid points and 19 blocks.
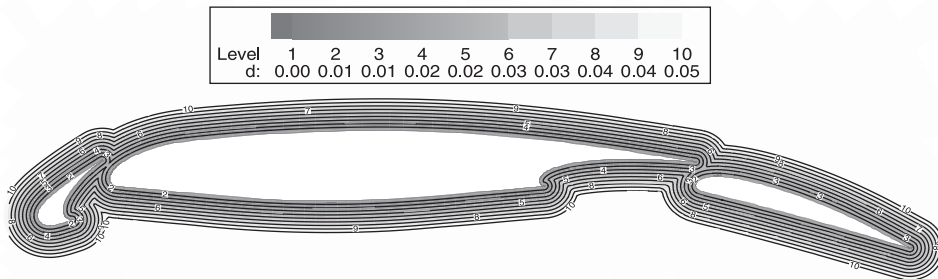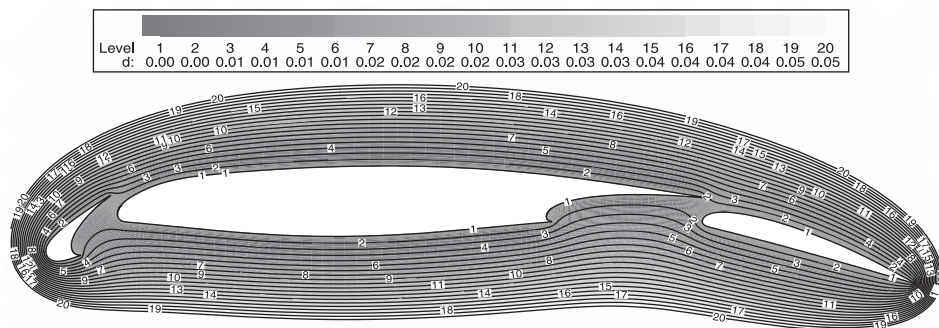
Figure 11. Exact distance.

Figure 12. Calculated distance with $\sigma = 1.0$ and $\mathcal{G}_0 = 1.0$.
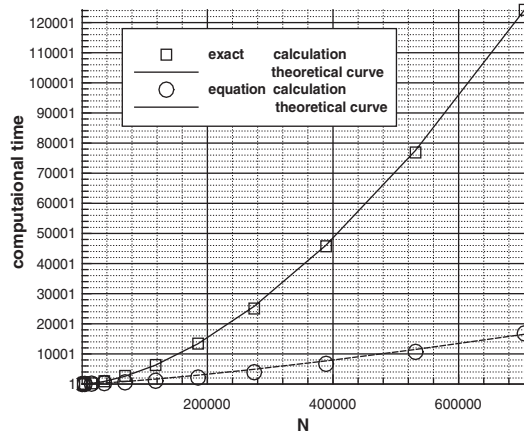
Figure 13. Computational time normalized by the time required for the
smallest grid with $9 \times 9 \times 9$ grid points.

the subdomains and the computational time T_{calc} within each subdomain. Considering a parallel machine, where T_{comm} is not negligible compared to T_{calc} and each subdomain is mapped to one CPU, the following approximations can be derived:

- exact distance

$$T_{\text{comm}} \sim K \cdot M \sim K \cdot N^{2/3} \qquad T_{\text{calc}} \sim (N/K) \cdot M \sim N^{5/3}/K \qquad (31)$$

- equation

$$T_{\text{comm}} \sim \text{it} \cdot B \sim \text{it} \cdot (N/K)^{2/3} \qquad T_{\text{calc}} \sim \text{it} \cdot N/K \qquad (32)$$

The number of iterations it needed for convergence are higher in the multi-block case compared to the one block case. The iterations range from $\text{it} = 41$ for $K = 8$ to $\text{it} = 87$ for $K = 125$. Approximating this behaviour by $\text{it} \sim K^a$ leads to $a \approx 0.3$. It is clear from Equations (31) and (32) that both high mesh resolution number or high subdivision favour the use of the proposed equation, since T_{comm} and T_{calc} have a lower scaling for the numerical solution of the differential equation. Figure 14 shows an example of the scaling with growing block and processor number, respectively. The run was done on a PC cluster with 16 nodes and two processors per node. The size of the problem N/K was equal for each processor. The exchange between the subdomains is optimised in both the exact calculation and the numerical solution to minimize communication and achieve load balancing.

5. CONCLUSION

A partial differential equation for the distance function to a surface is derived. This new formulation promises an enhancement of turbulence models at strong curved surfaces. Advantages over the direct calculation of the distance can be achieved on parallel computers
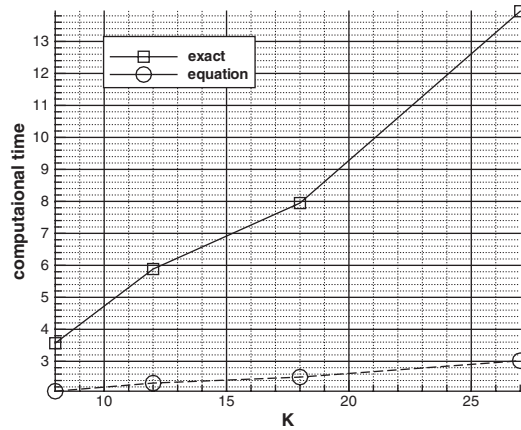
Figure 14. Computational time normalized by the time required for one block.

in terms of computational and communication times. Details about the numerical solution of the equation are presented and the method is applied to one- and two-dimensional examples. The impact of the two parameters σ and $\mathscr{G}_0$, that control the smoothing behaviour of the equation, is thoroughly investigated. The solution yields the exact normal distance in the case of the flat plate independent of the values chosen for these parameters. In the case of curved surfaces like corners or ellipses a smoothing can be enlarged by choosing a greater σ and/or a smaller value of $\mathscr{G}_0$. Furthermore they offer the possibility to control the near-wall behaviour. By assigning different values of $\mathscr{G}_0$ to different objects in the computational domain a further tuning of the opposing wall influence can be achieved. Further discussion of the coupling of the proposed equation and a turbulence model including the choice of the parameters is underway.

APPENDIX A

Equation

The proposed equation for the inverse distance $\mathscr{G}$ reads

$$(\mathscr{G} \cdot \mathscr{G}_x)_x + (\mathscr{G} \cdot \mathscr{G}_y)_y + (\mathscr{G} \cdot \mathscr{G}_z)_z + (\sigma - 1) \cdot \mathscr{G} \cdot (\mathscr{G}_{xx} + \mathscr{G}_{yy} + \mathscr{G}_{zz}) - \gamma \cdot \mathscr{G}^4 = 0 \qquad (A.1)$$

with

$$\sigma \gtrless 0.2 \qquad (A.2)$$

$$\gamma = (1 + 2\sigma) \qquad (A.3)$$

$$d = \frac{1}{\mathscr{G}} - \frac{1}{\mathscr{G}_0} \qquad (A.4)$$

Three special cases exist for two values of σ

- $\sigma = 0.0$ (exact distance)

$$(\mathcal{G} \cdot \mathcal{G}_x)_x + (\mathcal{G} \cdot \mathcal{G}_y)_y + (\mathcal{G} \cdot \mathcal{G}_z)_z - \mathcal{G} \cdot \left(\mathcal{G}_{xx} + \mathcal{G}_{yy} + \mathcal{G}_{zz}\right) - \mathcal{G}^4 = 0 \tag{A.5}$$

- $\sigma = 1.0$

$$(\mathcal{G} \cdot \mathcal{G}_x)_x + (\mathcal{G} \cdot \mathcal{G}_y)_y + (\mathcal{G} \cdot \mathcal{G}_z)_z - \gamma \cdot \mathcal{G}^4 = 0 \tag{A.6}$$

- $\sigma \rightarrow \infty$

$$\mathcal{G}_{xx} + \mathcal{G}_{yy} + \mathcal{G}_{zz} - 2\mathcal{G}^3 = 0 \tag{A.7}$$

Initial condition

$$\mathcal{G}_{\text{init}} = [0.0 \ldots 0.001] \cdot 1/x_{\text{ref}} \tag{A.8}$$

If for numerical reasons the value of 0 cannot be chosen to initialize the distribution then a very small value will be a good approximation for the free stream condition.

Boundary conditions
Wall

$$\mathcal{G}_{\text{wall}} = \mathcal{G}_0 \approx 1 \cdot 1/x_{\text{ref}} \tag{A.9}$$

Other values of $\mathcal{G}_0$ depending on the type of the wall are possible.

Far Field/inflow-outflow. The distance $\mathcal{D}$ is approximated at the boundary according to the following linear equation

$$\mathcal{D}^* = \frac{1}{\mathcal{G} + 1.0} \tag{A.10}$$

$$\mathcal{D}^* = a_0 + a_1 x + a_2 y + a_3 z \tag{A.11}$$

where the coefficients a_0, a_1, a_2 and a_3 are determined through the inversion of the 4×4 matrix

$$\begin{pmatrix} n & \Sigma x_i & \Sigma y_i & \Sigma z_i \\ \Sigma x_i & \Sigma x_i^2 & \Sigma x_i y_i & \Sigma x_i z_i \\ \Sigma y_i & \Sigma x_i y_i & \Sigma y_i^2 & \Sigma y_i z_i \\ \Sigma z_i & \Sigma x_i z_i & \Sigma y_i z_i & \Sigma z_i^2 \end{pmatrix} \begin{pmatrix} a_0 \\ a_1 \\ a_2 \\ a_3 \end{pmatrix} = \begin{pmatrix} \Sigma \mathcal{D}_i \\ \Sigma x_i \mathcal{D}_i \\ \Sigma y_i \mathcal{D}_i \\ \Sigma z_i \mathcal{D}_i \end{pmatrix} \tag{A.12}$$

where the sum Σ is carried out over $n \geqslant 3$ points from the interior of the integration domain. The approximating function (A.11) can be used to determine the value

$$\mathscr{G}_b = 1/\mathscr{D}_b^* - 1.0 \tag{A.13}$$

according to the grid co-ordinates of the boundary points. The value 1.0 is added to avoid division by zero ($\mathscr{D} = 1/\mathscr{G}$) at the beginning of the calculation. This type of boundary condition is also suitable for unstructured grids with the only limitation that the co-ordinates of the chosen approximating n points are not linearly dependent (e.g. do not lie on one line).

Discretization

The discretization is given for one direction (other directions are similar since the equation contains no cross derivatives)

$$[(\mathscr{G} \cdot \mathscr{G}_x)_x]_i = \frac{1}{x_{i+1} - x_{i-1}} \cdot \left(\frac{\mathscr{G}_{i+1}^2 - \mathscr{G}_i^2}{x_{i+1} - x_i} - \frac{\mathscr{G}_i^2 - \mathscr{G}_{i-1}^2}{x_i - x_{i-1}} \right) \tag{A.14}$$

$$[\mathscr{G} \cdot \mathscr{G}_{xx}]_i = \frac{2\mathscr{G}_i}{x_{i+1} - x_{i-1}} \cdot \left(\frac{\mathscr{G}_{i+1} - \mathscr{G}_i}{x_{i+1} - x_i} - \frac{\mathscr{G}_i - \mathscr{G}_{i-1}}{x_i - x_{i-1}} \right) \tag{A.15}$$

Jacobian for the Newton iteration

The complete Jacobian $\mathscr{J}$ is given for one direction at a constant time level n

$$\tilde{\mathscr{J}}_{ii-1} = \frac{2}{x_i - x_{i-1}}(\mathscr{G}_{i-1} + (\sigma - 1)\mathscr{G}_i) \tag{A.16}$$

$$\tilde{\mathscr{J}}_{ii} = -2\mathscr{G}_i \left(\frac{1}{x_{1+1} - x_i} + \frac{1}{x_i - x_{i-1}} \right)$$

$$+ 2(\sigma - 1) \left(\frac{\mathscr{G}_{i+1} - 2\mathscr{G}_i}{x_{i+1} - x_i} + \frac{\mathscr{G}_{i-1} - 2\mathscr{G}_i}{x_i - x_{i-1}} \right)$$

$$- 4(x_{i+1} - x_{i-1}) \cdot \gamma \mathscr{G}_i^3 \tag{A.17}$$

$$\tilde{\mathscr{J}}_{ii+1} = \frac{2}{x_{i+1} - x_i}(\mathscr{G}_{i+1} + (\sigma - 1)\mathscr{G}_i) \tag{A.18}$$

$$\mathscr{J}_{ij} = \frac{\tilde{\mathscr{J}}_{ij}}{x_{i+1} - x_{i-1}} \tag{A.19}$$

APPENDIX B:

NOMENCLATURE

B	number of grid points on multiblock boundaries
K	number of subdomains
M	number of grid points on the boundary
N	number of total grid points
T	computational time
it	number of iterations
$a, b, c,$	parameters used
a_0, a_1, a_2, a_3	in approximations
d, y	exact distance
Δd	difference between exact and calculated distance
k_s	wall roughness
c_r	relaxation factor
$\mathscr{D}$	distance function
σ	smoothing parameter
γ	factor of source term
$\mathbf{n}$	normal vector on surface
$\mathscr{G}$	inverse distance function
x_r, x_{ref}	reference length
x, y, z	cartesian co-ordinates
i, j, k	discrete indices in x, y, z directions
α, β	angles
r	distance to the co-ordinate origin
$\mathbf{r}$	position vector
$\mathscr{O}(\ )$	order
$\mathscr{R}$	residual
$\mathscr{J}$	Jacobian
∂_n	normal derivative
$(\ )^+$	sublayer scaled values
$(\ )^{\mathrm{T}}$	transpose
$(\ )^{-1}$	inverse of matrix
$(\ )_{x,y,z}$	first derivatives/component in the direction
$(\ )_{xx,yy,zz}$	second derivatives
$(\ )_{\mathrm{wall}}$	wall (surface) value
$(\ )_b$	boundary value
$(\ )_{\mathrm{in}}$	first inner value
$(\ )_{ijk}$	value at node i, j, k
$(\ )_0$	constant values
$(\ )_{\mathrm{ref}}$	reference value
$(\ )_{\mathrm{exact}}$	exact value
$(\ )_{\mathrm{calculated}}$	calculated value
$(\ )_{\mathrm{eff}}$	effective value
$(\ )_{\mathrm{init}}$	value used for initialization

$(\quad)_{diag}$ diagonal component of matrix

$(\quad)_{approx.}$ approximated value or function

$(\quad)_{calc}$ calculation time

$(\quad)_{comm}$ communication time

$(\quad)^{(n)}$ timelevel/iteration index n

$(\tilde{\quad})$ non-dimensional value

REFERENCES

1. Baldwin BS, Lomax H. Thin layer approximation and algebraic model for separated turbulent flows. *AIAA Paper*, 1978; 78–257.
2. Baldwin BS, Barth TJ. A one-equation turbulence transport model for high Reynolds number wall-bounded flows. *AIAA Paper*, 1991; 91–0610.
3. Spalart PR, Allmaras SR. A one-equation turbulence model for aerodynamic flows. *AIAA Paper*, 1992; 92-0439.
4. Shur M, Strelets M, Zaikov L, Gulyaev AN, Kozlov VE, Secundov AN. A comparative numerical testing of one- and two-equation turbulence models for flows with separation and reattachment. *AIAA Paper*, 1995; 95-0863.
5. Menter FR. Zonal two equation $k - \omega$ turbulence models for aerodynamic flows. *AIAA Paper*, 1993; 93-2906.
6. Tucker PG. Assessment of geometric multilevel convergence robustness and a wall distance method for flows with multiple internal boundaries. *Applied Mathematical Modelling* 1998; **22**:293–311.
7. Tucker PG. Prediction of turbulent oscillatory flows in complex systems. *International Journal for Numerical Methods in Fluids* 2000; **33**:869–895.
8. Fares E, Meinke M, Schröder W. Numerical simulation of the interaction of wingtip vortices and engine jets in the near field. *AIAA Paper*, 2000; 2000–2222.
9. Fares E, Meinke M, Schröder W. Numerical simulation of the interaction of flap side-edge vortices and engine jets. *ICAS Paper presented at ICAS 2000 Congress in Harrogate*, ICA 0212, 2000.
10. Menter FR, Grotjans H, Unger F. Numerical aspects of turbulence modelling for the Reynolds averaged Navier–Stokes equations. Unpublished work, ASC–Advanced Scientific Computing GmbH, Germany, 1999.
11. Lee J, Paynter GC. Modified Spalart–Allmaras one-equation turbulence model for rough wall boundary layers. *Journal of Propulsion*, Technical Notes, 1996; **12**(4):809–811.
12. Moir IRM. Measurements on a two-dimensional aerofoil with high-lift devices. *AGARD-AR-303*, 1994; **2**: 58–59.